2-3-2021

Enhanced efficacy and increased long-term toxicity of CNS-directed, AAV-based combination therapy for Krabbe disease

Yedda Li

Christopher A Miller

Lauren K Shea

Xuntian Jiang

Miguel A Guzman

See next page for additional authors

Authors

Yedda Li, Christopher A Miller, Lauren K Shea, Xuntian Jiang, Miguel A Guzman, Randy J Chandler, Sai M Ramakrishnan, Stephanie N Smith, Charles P Venditti, Carole A Vogler, Daniel S Ory, Timothy J Ley, and Mark S Sands

Enhanced Efficacy and Increased Long-Term Toxicity of CNS-Directed, AAV-Based Combination Therapy for Krabbe Disease

Yedda Li,[1] Christopher A. Miller,[1] Lauren K. Shea,[1] Xuntian Jiang,[1] Miguel A. Guzman,[2] Randy J. Chandler,[3] Sai M. Ramakrishnan,[1] Stephanie N. Smith,[3] Charles P. Venditti,[3] Carole A. Vogler,[2] Daniel S. Ory,[1] Timothy J. Ley,[1,4] and Mark S. Sands[1,4]

[1]Department of Medicine, Washington University School of Medicine, St. Louis, MO, USA; [2]Department of Pathology, St. Louis University School of Medicine, St. Louis, MO, USA; [3]Medical Genomics and Metabolic Genetics Branch, National Human Genome Research Institute, Bethesda, MD, USA; [4]Department of Genetics, Washington University School of Medicine, St. Louis, MO, USA

Infantile globoid cell leukodystrophy (GLD, Krabbe disease) is a demyelinating disease caused by the deficiency of the lysosomal enzyme galactosylceramidase (GALC) and the progressive accumulation of the toxic metabolite psychosine. We showed previously that central nervous system (CNS)-directed, adeno-associated virus (AAV)2/5-mediated gene therapy synergized with bone marrow transplantation and substrate reduction therapy (SRT) to greatly increase therapeutic efficacy in the murine model of Krabbe disease (Twitcher). However, motor deficits remained largely refractory to treatment. In the current study, we replaced AAV2/5 with an AAV2/9 vector. This single change significantly improved several endpoints primarily associated with motor function. However, nearly all (14/16) of the combination-treated Twitcher mice and all (19/19) of the combination-treated wild-type mice developed hepatocellular carcinoma (HCC). 10 out of 10 tumors analyzed had AAV integrations within the *Rian* locus. Several animals had additional integrations within or near genes that regulate cell growth or death, are known or potential tumor suppressors, or are associated with poor prognosis in human HCC. Finally, the substrate reduction drug L-cycloserine significantly decreased the level of the pro-apoptotic ceramide 18:0. These data demonstrate the value of AAV-based combination therapy for Krabbe disease. However, they also suggest that other therapies or co-morbidities must be taken into account before AAV-mediated gene therapy is considered for human therapeutic trials.

INTRODUCTION

Infantile globoid cell leukodystrophy (GLD, Krabbe disease) is a rapidly progressive and invariably fatal lysosomal storage disorder caused by the deficiency of galactosylceramidase (GALC) activity.[1] Symptoms typically appear by 3–6 months of age, and death occurs by 2–4 years of age. GALC deficiency results in the rapid accumulation of psychosine, a toxic glycolipid normally degraded by GALC in the lysosome.[2] Psychosine accumulates in all cell types, but most rapidly in oligodendrocytes and Schwann cells, leading to profound demyelination. Krabbe disease is characterized by failure to thrive, limb stiffness, weakness, paralysis, blindness, and developmental delay and regression. Currently, the only available therapy is hematopoietic stem cell transplantation (HSCT), which must be administered prior to symptom onset to delay progression.[3] This treatment is not curative.

The Twitcher (Twi) mouse is a genetically faithful model of Krabbe disease that closely parallels the biochemical, histological, and clinical progression of the human disease. Twi mice experience a rapidly progressive disease course, with tremors and ataxia starting at ∼25 days and death occurring by ∼40 days.[4,5] The Twi mouse has been an indispensable tool for testing new therapies. However, finding an effective therapy has been a challenge. The majority of single modality therapies provide only limited clinical benefit and none are curative.[6–8] Several groups have shown that combination therapies targeting multiple pathogenic mechanisms result in dramatic clinical improvements.[9–13]

We showed previously that early intervention (newborn) with central nervous system (CNS)-directed, adeno-associated virus 2/5 (AAV2/5)-mediated gene therapy synergized with HSCT to increase the median lifespan (∼110 days) of Twi mice to a greater extent than the sum of the increases from the individual treatments.[10] We subsequently showed that the synergy was likely due to AAV-mediated gene therapy supplying a persistent source of the deficient enzyme while HSCT provided a significant immunomodulatory effect.[14] Although this combination represented a significant advance, the increase in lifespan was modest compared to the lifespan of a normal laboratory mouse. Therefore, we added a small-molecule substrate reduction therapy (SRT) drug, L-cycloserine, to the AAV2/5 gene therapy/HSCT regimen.

L-cycloserine inhibits serine palmitoyl transferase, an enzyme upstream of psychosine synthesis, and has been shown to slow psychosine accumulation.[15] The addition of thrice weekly injections of L-cycloserine dramatically and synergistically increased the median lifespan of Twi mice to ~300 days.[16] Despite the improvements in lifespan, correction of motor deficits (rotarod and wirehang) remained incomplete.

As we systematically tested various combination approaches, the second-generation AAV2/5 vector remained constant. In the current study, we performed the same triple-treatment (3xRx) experiment as described above using the same recombinant AAV genome but packaged with an AAV9 capsid.[17] This newer generation AAV vector further increased efficacy. The median lifespan of 3xRx Twi mice was increased to ~400 days. Importantly, the clinical/behavioral deficits dramatically improved, and in some cases, completely normalized for the entire life of the animal. Unexpectedly, most of the 3xRx Twi mice did not appear to die from Krabbe disease. Rather, they likely succumbed to hepatocellular carcinoma (HCC) later in life. Nearly 90% (14/16) of the 3xRx Twi mice and 100% (19/19) of the 3xRx normal control mice had large hepatic tumors when necropsied. In fact, it was difficult to identify normal-appearing liver in several of the animals.

Hepatocellular carcinoma has been reported by several groups at ≥1 year of age following intravenous injection of AAV vectors in newborn mice.[18–21] To our knowledge, HCC has never been reported following CNS-directed, AAV-mediated gene therapy. Although the exact cause of HCC in the current study is not known, our data suggest that AAV integration into the *Rian* locus represents one "hit" in the "multi-hit" process leading to cancer.[22] Sequence analysis suggested that secondary AAV integrations may have provided additional events that cooperated to cause HCC. Finally, L-cycloserine may have also contributed to the development of HCC by decreasing the levels of the anti-proliferative and pro-apoptotic ceramide 18:0,[23] a ceramide species that is downregulated in human HCC cells.[24]

In total, these data show that combination therapy is a highly effective treatment for murine GLD. However, our findings also raise concerns for the use of high doses of very efficient AAV vectors in combination with drugs or approaches that may have oncogenic potential.

RESULTS

Lifespan
Twi mice received intracranial (IC) and intrathecal (IT) injections of AAV2/9-GALC at birth alone (Twi AAV2/9-GALC), in combination with HSCT at postnatal day (PND) 2 (Twi 2xRx), or in combination with HSCT and thrice weekly SRT with L-cycloserine (Twi 3xRx). Groups of untreated wild-type (WT) and Twi mice, as well as 3xRx WT animals, were also generated. These animals were analyzed biochemically and histologically at 36 days of age and at a terminal time point, as well as functionally for lifespan and motor function.

Untreated Twi mice had a median lifespan of 41 days (range: 24–46 days; Figure 1A). Twi mice treated with AAV2/9-GALC alone, AAV2/9-GALC + HSCT (2xRx), and AAV2/9-GALC + HSCT + L-cycloserine (3xRx) had median lifespans of 66.5 days (range: 50–83 days), 269 days (range: 180–673 days), and 404 days (range: 157–569 days), respectively. Although the median lifespan of the 2xRx Twi mice was more than 4 months less than the 3xRx Twi mice, they were not significantly different. WT mice treated with the same 3xRx regimen had a median lifespan of 440 days (range: 347–507 days). All untreated WT mice lived to at least 673 days, at which point they were sacrificed to terminate the study.

Body Weight
Untreated Twi mice fail to thrive, as indicated by severely impaired weight gain and a mean maximum weight of 7.8 ± 0.5 g (Figure 1B). Both 2xRx and 3xRx combination therapies improved weight gain, with body weights plateauing at a mean of ~18 g for both groups. WT mice receiving 3xRx therapy reached a mean weight of ~21 g, which was significantly less than that of untreated WT animals (>30 g).

Motor Function
Motor function was assessed by rotarod (Figures 1C and 1D) and wirehang (Figure 1E) tests. Untreated Twi mice were unable to complete the rotarod or the wirehang test at 4 weeks of age. Untreated WT mice performed both rotarod and wirehang for 60 s (the maximum tested time) throughout life. Twi mice treated with 2xRx therapy were able to perform rotarod at near-WT levels until approximately 1 month prior to death, after which their performance rapidly deteriorated. Nearly all 3xRx-treated Twi mice performed the rotarod test at WT levels throughout life and were able to maintain a 60 s performance until they were moribund (Figure 1D).

Untreated Twi mice are not able to perform the wirehang at any point in their lives (Figure 1E).[16] Twi mice receiving 2xRx therapy were able to perform the wirehang test at near-WT levels until 10 weeks of age, after which their wirehang performance quickly deteriorated. No 2xRx Twi mouse was able to stay on the inverted wire for 60 s past 90 days (12 weeks). At 10 weeks of age, Twi mice receiving 3xRx therapy were able to perform the wirehang at near-WT levels. At every subsequent time point, 3xRx-treated Twi mice performed significantly better on the wirehang than 2xRx-treated Twi mice. Some 3xRx-treated Twi mice were able to perform the wirehang test for the full 60 s at 60 weeks of age.

Biochemical Analyses
The brains of Twi mice had virtually undetectable levels of GALC activity when compared to that of their WT littermates (Figure 2A). All mice treated with AAV2/9-GALC gene therapy, either as a single therapy or in combination, had at least physiologic levels of GALC activity that persisted for the life of the animals. There was no significant difference in brain GALC activity between animals receiving AAV2/9-GALC alone, 2xRx therapy, or 3xRx therapy, suggesting that neither HSCT nor SRT contributed to the increase in GALC activity in treated Twi mice.

For both brain (Figure 2B) and sciatic nerve (Figure 2C), psychosine levels were significantly and persistently decreased in AAV2/9-GALC
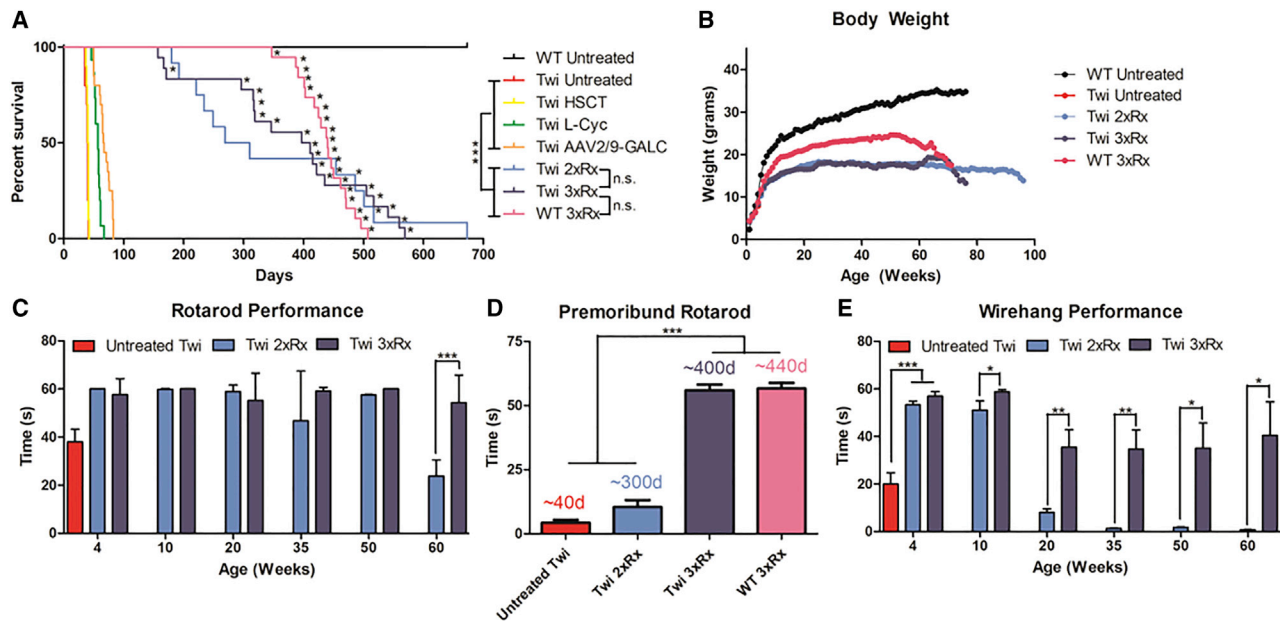
Figure 1. Triple Combination Therapy Increases Lifespan and Improves Clinicobehavioral Performance in Twi Mice

(A) Kaplan-Meier curves showing increased lifespan in 3xRx Twi mice (n = 16), 2xRx Twi mice (n = 14), and AAV2/9-GALC alone Twi mice (n = 25) compared to untreated Twi mice (n = 10). WT mice treated with 3xRx therapy (n = 19) had a significantly shorter lifespan than untreated WT mice (n = 11). Asterisks indicate mice that had large hepatocellular carcinoma tumors at death. The lifespan data for Twi mice treated with HSCT or L-cycloserine alone are from previous publications[10,16] and shown as a comparison for monotherapy animals. (B) Combination therapies improve weight gain in Twi mice but cause weight loss in WT mice. Untreated Twi mice (Twi untreated) have profoundly impaired weight gain compared to WT mice (WT untreated). Double (Twi 2xRx) and triple (Twi 3xRx) combination therapy partially improve weight gain in Twi mice, but WT mice receiving 3xRx therapy (WT 3xRx) have mildly impaired weight gain compared to untreated WT mice. (C) Rotarod testing shows nearly normal performance in 3xRx-treated Twi mice (Twi 3xRx) throughout life. Twi 2xRx also significantly improves rotarod performance. However, 2xRx Twi mice eventually are unable to remain on the rotarod. In contrast, only a few untreated Twi (untreated Twi) mice are able to stay on the rotating rod for the full 60 s, even early in life, and are dead by 5–6 weeks of age. (D) Premoribund rotarod performance was assessed 1–7 days prior to death. Twi mice treated with 3xRx therapy perform as well as untreated WT (data not shown) and 3xRx-treated WT mice (WT 3xRx) up until death. In contrast, untreated Twi mice and 2xRx-treated Twi mice can no longer perform rotarod when premoribund. The median age at premoribund testing for mice in each experimental group is indicated above the corresponding column. (E) 2xRx and 3xRx Twi mice have near-normalized wirehang performance at 10 weeks of age. Although performance is impaired at subsequent time points, 3xRx-treated Twi mice perform significantly better than 2xRx-treated Twi mice at every time point starting at 10 weeks. Untreated WT mice are able to remain on the wirehang for 60 s throughout life. The error bars represent one standard error of the mean, *p < 0.05, **p < 0.01, ***p < 0.005.

only, 2xRx, and 3xRx Twi mice, compared to untreated Twi mice. There was no significant difference in brain or sciatic nerve psychosine levels between mice treated with AAV2/9-GALC alone, 2xRx therapy, or 3xRx therapy. However, a slight elevation in psychosine was detected in both the brain and sciatic nerves in the treated Twi mice compared to WT mice at nearly every time point.

Donor Cell Engraftment

Twi mice treated with 2xRx or 3xRx therapy had mean GFP[+] donor engraftment levels of 52.9% ± 19.9% and 46.9% ± 20.2%, respectively. WT mice treated with 3xRx therapy had a mean engraftment level of 44.6% ± 18.0%. There is no significant difference in engraftment between these three groups (Figure 2D).

Peripheral Neuropathy

Untreated Twi mice had fewer axons, significant peri-axonal edema, and macrophage infiltration in the sciatic nerve compared to WT mice (Figures 3A–3D). Twi mice receiving 3xRx therapy had significant

albeit incomplete correction of peripheral nerve structure, with fewer infiltrating monocytes/macrophages, less peri-axonal edema, and significantly more axons (Figure 3E) than age-matched untreated Twi mice. Sciatic nerve pathology was not corrected in 36-day-old 2xRx Twi mice.

Neuroinflammation

Twi mice had profound and global microgliosis (CD68^{+}; Figure 4) compared to WT mice. The hindbrain (cerebellum and brain stem) was more severely affected than the forebrain (cortex). Both 2xRx and 3xRx therapy attenuated microgliosis in Twi mice at 36 days of age. However, CD68 staining increased in both 2xRx and 3xRx Twi mice as they aged. Whole-brain homogenates showed significant elevations in G-CSF (Figure 5A), KC (Figure 5B), MCP-1 (Figure 5C), and MIP-1α (Figure 5D) in untreated 36-day-old Twi mice compared to their WT littermates. Although CNS-directed, AAV-mediated gene therapy alone initially decreased the levels of cytokines/chemokines, it failed to maintain these levels in aged mice. In contrast, both
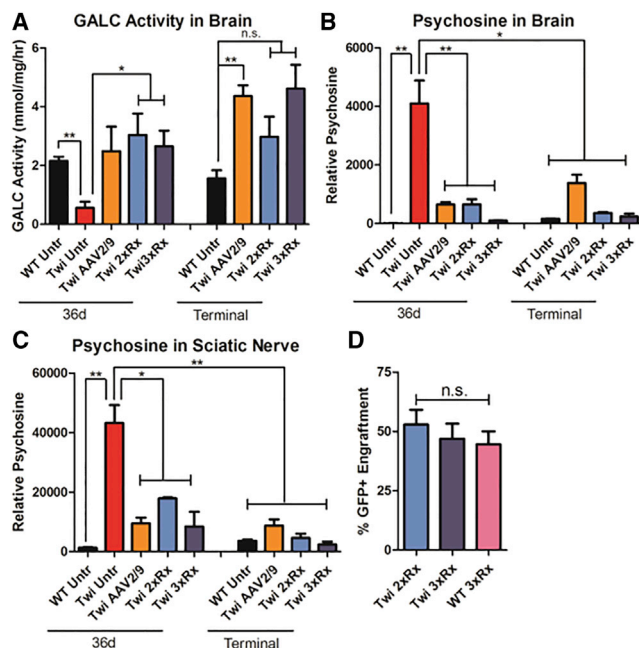
Figure 2. Combination Therapies Normalize Biochemical Features of Murine Krabbe Disease

(A) GALC activity is deficient in untreated Twi brains (Twi Untr). Compared to untreated WT mice (WT Untr), Twi mice treated with AAV2/9-GALC alone (Twi AAV2/9), 2xRx therapy (Twi 2xRx), and 3xRx therapy (Twi 3xRx) have at least physiologic levels of GALC activity in the brain. Psychosine levels in (B) brain and (C) sciatic nerve are much higher in Twi Untr mice compared to WT Untr mice and Twi mice treated with AAV2/9-GALC alone, 2xRx therapy, or 3xRx therapy. All therapies significantly decrease psychosine accumulation in brain and sciatic nerves throughout the lives of Twi mice. (D) There is no significant difference in donor (GFP+) bone-marrow engraftment between Twi or WT mice receiving 2xRx or 3xRx therapies. The error bars represent one standard error of the mean, *p < 0.05, **p < 0.01.

2xRx and 3xRx therapy normalized cytokine/chemokine expression in the brain for the life of the animals.

Hepatocellular Carcinoma

We observed hepatic tumors (Figure 6A) in 14/16 3xRx Twi mice, 2/14 2xRx Twi mice, and 19/19 3xRx WT mice (Figure 6B). We performed targeted sequence capture analyses on genomic DNA from tumor and normal-appearing liver tissue from 10 WT animals receiving 3xRx in order to identify potential AAV integration sites. 82 capture probes were generated that spanned the entire AAV vector, including the inverted terminal repeats (ITRs), the CAGGS promoter, and the human GALC cDNA. After capture and sequencing, the data were aligned to the mm10 reference genome with the AAV vector sequence appended. Integration sites were defined by taking reads aligned to the AAV sequence and finding regions where the paired reads mapped recurrently. There were ~73 unique integration events that met these strict criteria (Table S1). As an indicator that the targeted sequence capture method faithfully identified the correct sequences, every exon of the murine Galc gene was detected in tumor and normal-appearing tissue with read counts ranging from single digits to hundreds (Figure S1).

Tumors from all (10/10) of the animals had AAV integrations within the Rian locus (Table 1; Figure S2A). Although several AAV integration events occurred near miR-341, none were present within that microRNA (Figure 7). The integrated vectors largely appeared to be rearranged such that the identified break points within the integrated AAV sequences occurred in the 5′ portion of the vector (Table S2). Several animals had additional AAV integrations in or near genes associated with HCC and other malignancies (Akap13;[25] Figures S2B and S2C), that affect cell growth or death (Kcnh1[26] and Eva1a;[27] Figures S2D and S2E), or that are tumor suppressors (Foxp1,[28,29] Tusc3,[30] Magi1;[31,32] Figures S2F and S2G). In fact, one animal (6675) with an integration in Rian also had intragenic integrations in both Foxp1 and Tusc3, which are known and candidate tumor suppressors, respectively.

Since the penetrance of HCC was much lower in 2xRx compared to 3xRx Twi mice, we hypothesized that L-cycloserine might exacerbate the HCC predisposition imposed by AAV integrations. L-cycloserine significantly decreased the levels of the pro-apoptotic ceramide $18:0^{23,24}$ in tumor tissue compared to normal-appearing liver tissue (Figure 6C). However, there were no hepatic tumors observed in 11 out of 11 WT mice receiving thrice weekly subcutaneous injections of L-cycloserine alone for 1 year.

DISCUSSION

GLD is a rapidly progressing, demyelinating inborn error of metabolism for which there is currently no cure. Although GLD is a simple monogenic disorder, it has remained largely refractory to treatment.[8] This is likely due to the presence of multiple secondary pathogenic mechanisms arising from the primary GALC deficiency. In this study, we treated Twi mice with a triple therapy regimen that simultaneously targeted three major mechanisms. Central nervous system-directed AAV2/9-mediated gene therapy results in persistent, high levels of GALC activity. Hematopoietic stem cell transplantation ameliorates neuroinflammation.[14] L-cycloserine is a small-molecule drug that slows psychosine accumulation by inhibiting serine palmitoyl transferase, an enzyme that catalyzes an early step in ceramide synthesis.[15] This combination therapy resulted in a 10-fold increase in median lifespan of Twi mice. The synergistic effects of combination therapy in the current study are consistent with, but greater in magnitude than previous combination therapy studies.[9–14,16] It will be important to determine whether the synergy observed in the Twi mouse will translate to larger animal models of Krabbe disease.[37,38]

Another aspect of GLD that has remained relatively refractory to treatment is motor dysfunction, which is quantified in this study by the rotarod and wirehang tests. As performed in this study, rotarod primarily measures coordination, whereas wirehang is an indicator of peripheral neuropathy, limb strength, and coordination. While previous therapy studies have reported some improvements in both rotarod and wirehang performance,[11,16,39] improvements have been incomplete and/or limited, with mice falling off both apparatuses as the disease progresses. In the current study, 3xRx-treated Twi mice
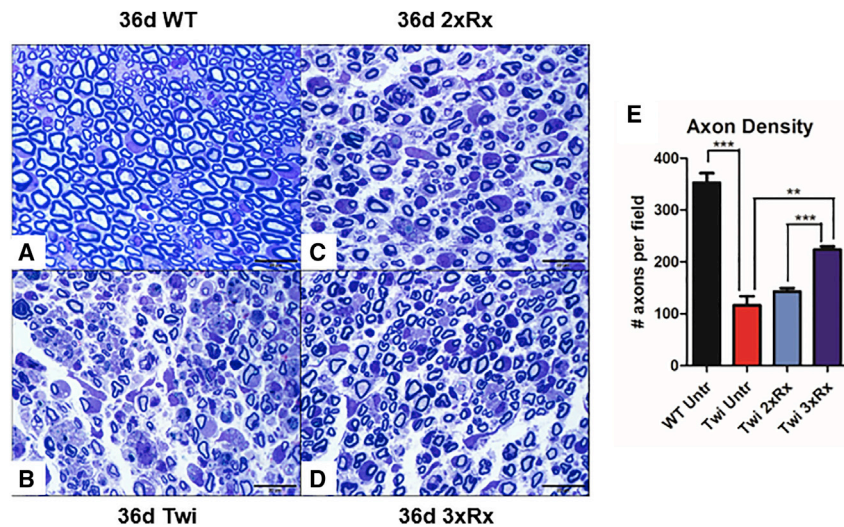
Figure 3. Combination Therapy Significantly Delays Progression of Sciatic Nerve Pathology

Compared to (A) 36-day-old WT mice (36d WT), (B) untreated Twi mice (36d Twi) have severe sciatic nerve pathology with decreased myelination, periaxonal edema, profound axonal degeneration, and macrophage infiltration. (C) 36-day 2xRx is less effective than (D) 36-day 3xRx at preserving overall sciatic nerve architecture in 36-day-old Twi mice. (E) Twi Untr mice have decreased axon density in the sciatic nerve. Twi 3xRx is significantly more effective than Twi 2xRx at preventing axonal loss. The error bars represent one standard error of the mean, **p < 0.01, ***p < 0.005.

were able to stay on the rotarod even when they were a few days from being moribund.

The wirehang test appears to be a more challenging exercise for Twi mice since untreated Twi mice cannot perform the task for 60 s at any point in their lives, and treated mice fail this test prior to failing on the rotarod.[16] Interestingly, half of the Twi mice receiving 3xRx therapy were able to perform wirehang for the maximal time tested (60 s) throughout life. In contrast, no 2xRx Twi mouse was able to perform the wirehang test for 60 s past 12 weeks of age. These data suggest that L-cycloserine plays an important role in correcting the peripheral neuropathy in Twi mice. This is supported by the greater histopathological improvements observed in the sciatic nerves of 3xRx-treated mice compared to 2xRx-treated mice.

Despite the significant improvement in lifespan and motor function, Twi mice treated with 3xRx therapy retain some signs of GLD, including a milder but persistent tremor and hind limb clasping. One potential explanation for continued disease progression is the uneven distribution of AAV2/9-mediated gene expression in the CNS and PNS, which has been described in other studies.[17] Although GALC levels were at least physiologic and psychosine accumulation was significantly reduced in whole-brain lysates of 3xRx-treated Twi mice, it is possible that uneven distribution of GALC expression resulted in focal areas of pathologic psychosine accumulation and continued, albeit slower, disease progression.

Another potential cause of GLD progression is the slow but worsening neuroinflammation in the treated Twi CNS. Untreated Twi mice have profound microgliosis and astrocytosis, as well as significantly increased expression of pro-inflammatory cytokines as early as postnatal day 2.[40,41] Cytokine/chemokine levels were normalized transiently and persistently in 2xRx- and 3xRx-treated Twi mice, respectively. However, the increased immunohistochemical staining for CD68 as combination-treated Twi mice age suggests that the cellular response is more refrac-

tory than the cytokine response. Alternatively, elevated cytokine levels in localized regions of the CNS may be masked when performing cytokine assays on whole-brain homogenates. Finally, psychosine accumulation in microglia and astrocytes has been hypothesized to directly activate these cells.[42] Therefore, it is possible that the low but persistent levels of psychosine in the CNS activate neuroinflammatory cells and contribute to the continued progression of disease.

In total, these data suggest that the 2xRx treatment regimen is less effective than the 3xRx approach and the 2xRx mice eventually succumb to Krabbe disease. In contrast, the addition of SRT to CNS-directed gene therapy and HSCT (3xRx) is much more effective. In fact, the 3xRx Twi mice did not appear to die from Krabbe disease. Rather, at death, the 3xRx Twi mice had a very mild Twi phenotype but nearly all of the mice had advanced HCC. 3xRx WT mice also had a dramatically shortened lifespan and all of the animals had advanced HCC.

It is clear that systemic delivery of an AAV vector to newborn mice can cause HCC.[33,43] However, to our knowledge, HCC has never been reported following CNS-directed, AAV-mediated gene transfer, even when using broadly trophic capsids such as AAV9. The incidence of HCC in both the 3xRx Twi and 3xRx WT mice in the current study approached 100%. In contrast, there was no evidence of HCC in a nearly identical study (same HSCT protocol and identical dose of L-cycloserine) in Twi mice using an AAV2/5 vector.[16] We hypothesize that leakage of the virus into the systemic circulation and the use of a more potent AAV vector contributed to the development of HCC. It has been shown by several groups that AAV vectors can "leak" into the systemic circulation following an IT injection and result in liver transduction that equals or exceeds CNS transduction.[44,45] It should be noted that the animals in the current study received both IC and IT injections of AAV. It should also be noted that vectors packaged in an AAV9 capsid transduce the liver 50- to 100-fold more efficiently than vectors packaged in an AAV5 capsid.[46]

We also hypothesize that one or both of the adjunct treatments used in this study (HSCT with pre-conditioning irradiation and L-cycloserine) greatly exacerbated the HCC phenotype and increased its penetrance. Our belief that several independent factors cooperated
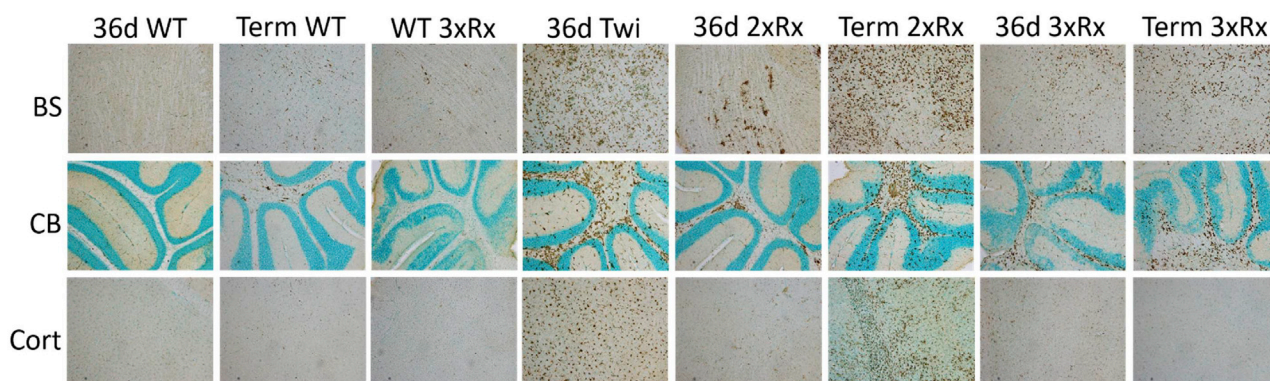
Figure 4. 3xRx Attenuates Microgliosis Early in the GLD Disease Course

Anti-CD68 immunohistochemistry shows profound microglial activation (brown staining) in untreated Twi (36d Twi) brainstem (BS), cerebellum (CB), and cortex (Cort). 36-day 2xRx Twi decreases microgliosis at 36 days but is unable to prevent eventual disease progression and development of severe neuroinflammation at a terminal time point (Term 2xRx). Microgliosis in terminal 3xRx-treated Twi mice (Term 3xRx) is less severe than that in Term 2xRx mice, especially in the cortex. Aging WT brains (Term WT) develop mild microglial activation throughout the brain.

to increase the incidence of HCC is consistent with Knudson's hypothesis stating that cancer results from the accumulation of multiple "hits" to the genome.[22] Ionizing irradiation generates double-stranded DNA breaks and small genomic insertions and deletions.[47] This could affect the rate or site preference for AAV integration. Aberrant ceramide levels have previously been reported in HCC. Specifically, C18:0 ceramide, which is anti-proliferative[23] and downregulated in human HCC,[24] is also downregulated in murine HCC tissue in the current study. The SRT used in this study, L-cycloserine, not only decreases the accumulation of the toxic metabolite psychosine, but it also reduces the levels of upstream lipids including ceramides. Interestingly, very few of the 2xRx animals (no L-cycloserine) developed HCC, and most of those animals lived well beyond 200 days. Although not definitive, this result suggests that the altered ceramide levels may play a role in the exacerbated HCC phenotype. Taken together, these data strongly suggest that ionizing irradiation and L-cycloserine administration may represent additional events that increase the likelihood of malignant transformation. However, it seems unlikely that the radiation and L-cycloserine by themselves result in HCC, at least within the time frame of this study, since there was no evidence of HCC in the nearly identical study cited above.[16] The only known difference between the prior and current studies is the use of an AAV2/9 rather than AAV2/5 vector, suggesting that the more potent AAV2/9 vector is necessary for the high penetrance of HCC. Finally, it has been suggested that the presence of a reporter gene (e.g., GFP) might increase the toxicity of AAV-mediated gene therapy.[48] In the current study, GFP is constitutively expressed from a stable transgene in the donor hematopoietic-derived cells in order to determine engraftment. It is formally possible that GFP expression in donor-derived fixed tissue macrophages in the liver (Kupfer cells) may contribute to the development of HCC through a bystander effect.

Targeted sequence capture using probes specific for the AAV vector showed that tumors from 90% of the animals analyzed had AAV in-

tegrations in the *Rian* locus. This is not surprising, since it is known that tumors in mice treated during the neonatal period are associated with AAV vector integration in the *Rian* locus.[19,33] Interestingly, the integrated AAV vectors isolated from the tumors are typically rearranged such that the 5′ ITR and *cis*-acting regulatory elements are intact but the 3′ sequences, including the transgene of interest, are deleted. Consistent with these findings, the vectors integrated into the *Rian* locus in the current study appear to be rearranged in a similar manner such that the 5′ sequences are the predominant sequences identified. It has been shown previously that these rearranged vectors dysregulate the *Rian* locus and downstream genes. In fact, prior experiments using an integrating AAV containing only the chicken β-actin (CBA) promoter have proven that dysregulation of the *Rian* locus represents an initiating event that is sufficient to cause clonal expansion and transformation in mouse hepatocytes.[33] The *Rian* locus is complex and encodes a number of genes, long noncoding RNAs, small RNAs, and microRNAs, one of which, *miR-341*, has been noted to be recurrently targeted in AAV-associated HCCs. Because this gene is unique to rats and mice and harbors nearly 60% of all the previously reported AAV integrations in the *Rian* locus, it might suggest that some genotoxic events are not necessarily translatable across species.

None of the integration events we captured map to *miR-341*. Integrations in the *Rian* locus in the current study are generally dispersed across the locus, mapping in between, and/or close to, the locations of other AAV integration events that have been previously reported with different vectors and animal models (Figure 7). In addition, several animals with integrations in *Rian* had additional AAV integrations into genes that regulate cell growth or cell death, or are associated with various malignancies, including HCC. Of particular interest is the fact that one animal (6675) had integrations not only in the *Rian* locus, but also in a known tumor suppressor gene (*Foxp1*) and a candidate tumor suppressor gene (*Tusc3*). Dysregulated expression of *Foxp1* has been associated with large tumor size, high serum
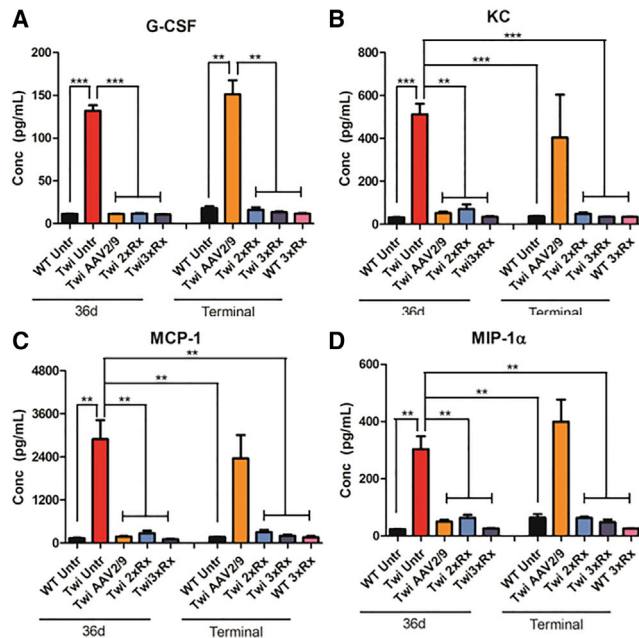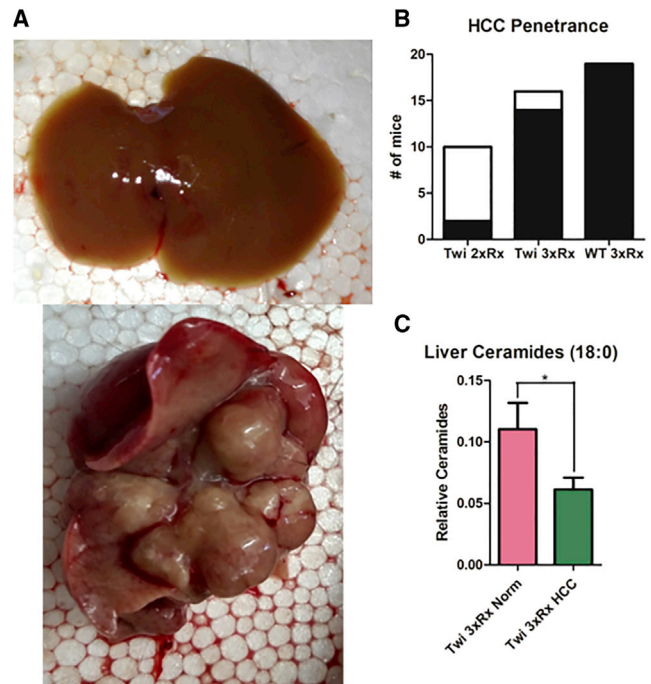
Figure 5. Combination Therapies Normalize Cytokine Expression in the Twi Brain

(A) G-CSF, (B) KC, (C) MCP-1, and (D) MIP-1α are significantly elevated in Twi Untr brains at 36 days of age. Gene therapy alone (Twi AAV2/9) decreases the expression of these cytokines at 36 days. However, by the time these mice are terminal, cytokine expression in Twi mice receiving AAV2/9 alone no longer differs from that of 36-day-old Twi Untr mice. Both 2xRx (Twi 2xRx) and 3xRx (Twi 3xRx) therapies normalize cytokine expression for the life of the animals. The error bars represent one standard error of the mean, **p < 0.01, ***p < 0.005.

Figure 6. 3xRx Significantly Increases the Penetrance of AAV-Induced HCC in Twi and WT Mice

(A) Representative images of gross normal liver (top panel) and HCC tumor (bottom panel) isolated from a terminal 3xRx-treated mouse. (B) The incidence of HCC (black fill) is increased in 3xRx-treated Twi (Twi 3xRx) and WT (WT 3xRx) mice compared to 2xRx-treated Twi mice (Twi 2xRx). (C) The level of the pro-apoptotic ceramide, 18:0, is significantly lower in tumor tissue (Twi 3xRx HCC) compared to normal-appearing liver tissue (Twi 3xRx Norm). The error bars represent one standard error of the mean, *p < 0.05.

α-fetoprotein levels, and poor prognosis in human HCC.[29] Low levels of *Tusc3* expression is an independent risk factor for overall and disease-free survival in human HCC.[30] Another animal (6902) with a Rian integration also had an insertional event in a different candidate tumor suppressor, *Magi1*, the downregulation of which has been associated with multiplicity of tumor nodules and poor clinical prognosis in human HCC.[32] Further studies will be necessary to determine whether those integration events acted as cooperating mutations that contributed to the development of AAV-mediated HCC.

The 3xRx combination therapy used in this study is a very effective therapy for Krabbe disease. Not only does it increase lifespan, but it also improves motor function in Twi mice. However, the administration of this therapy was not without risks. AAV-induced HCC in mice is a reproducible finding.[43] Insertional mutagenesis by WT AAV2 has also been implicated in the development of human HCC, albeit at a much lower rate than that observed in mice injected with recombinant AAV.[49] In addition, no AAV integrations have been identified in the syntenic *Rian* locus of the human genome in human HCC. There is a clear need to understand the role of AAV in the development of HCC and to determine how other therapies or co-morbidities might interact with AAV to increase the penetrance of HCC. In the specific case of Krabbe disease, less toxic conditioning regimens

and more precise SRT drugs will likely be necessary before a similar combination treatment regimen can be safely administered to affected children.

MATERIALS AND METHODS

Experimental Animals and Treatment Groups

Animals were housed at Washington University in St. Louis under the supervision of M.S.S. Heterozygous Twi ($GALC^{+/-}$) mice on a C57BL/6J background (Jackson Laboratory, ME, USA) were bred and maintained. Genotypes of all experimental mice were determined by PCR, as previously described.[50,51] Mice were housed under standard conditions, on a 12 h/12 h light/dark cycle with *ad libitum* access to food and water. HSC donors were syngeneic $GALC^{+/+}$ mice that expressed GFP under the CAG promoter.[52] All animal procedures were approved by the Institutional Animal Studies Committee at Washington University School of Medicine and were in accordance with the guidelines of the National Institutes of Health.

There were four treated and two untreated groups of animals in this study. The 3xRx Twi group was composed of 22 animals (16 for lifespan, behavior, and terminal histology; 3 for 36-day biochemistry

Table 1. AAV Integration Sites in or near Cancer- and Cell-Growth/Death-Associated Genes

Animal ID	Age[a] (months)	Chr	Integration[b] Start Site (bp)	Read Counts	Gene	Gene Description	Reference
6657	13.4	12	109643597[c]	857	*Rian*	microRNA cluster	[33]
6675	14.7	12	109618074[c]	1,390	*Rian*	microRNA cluster	[33]
		6	99150006[c]	4,883	*Foxp1*	Forkhead protein, tumor suppressor	[28,29]
		8	39104763[c]	199	*Tusc3*	endoplasmic reticulum (ER) protein, candidate tumor suppressor	[30]
6722	17.6	12	109631801[c]	3,060	*Rian*	microRNA cluster	[33]
		7	75627402[c]	1,682	*Akap13*	A-kinase anchor protein, double oncogene homology, breast cancer	[25,34]
6815	14.7	12	109609803[c]	1,684	*Rian*	microRNA cluster	[33]
6824	15.0	12	109631309[c]	213	*Rian*	microRNA cluster	[33]
		1	192215900[c]	55	*Kcnh1*	K^+ channel, increased expression confers growth advantage	[26,35]
		6	81973046[d]	87	*Eva1a*	regulator of programmed cell death	[27,36]
6828	13.1	12	109625075[c]	3,737	*Rian*	microRNA cluster	[33]
6902	14.9	12	109613953[c]	85	*Rian*	microRNA cluster	[33]
		12	109671965[e]	825	*Rian*	microRNA cluster	[33]
		6	94142817[c]	65	*Magi1*	membrane-associated guanylate kinase, candidate tumor suppressor	[31,32]
7025	15.5	12	109615046	1,430	*Rian*	microRNA cluster	[33]
7045	16.8	12	109606198[c]	3,519	*Rian*	microRNA cluster	[33]
7046	14.2	12	109611352[c]	387	*Rian*	microRNA cluster	[33]

[a]The age when the animals died or were sacrificed for humane reasons.
[b]The start and stop sites for each AAV integration are listed in Table S1.
[c]Intragenic integration site.
[d]Integration site ~60 kb upstream of *Eva1a*.
[e]Integration site ~15 kb downstream of *Rian*.

and histology; and 3 for 36-day cytokine analysis). The 2xRx Twi group was composed of 20 animals (14 for lifespan, behavior, and terminal histology; 3 for 36-day biochemistry and histology; and 3 for 36-day cytokine analysis). The AAV2/9-GALC treated Twi group (Twi AAV2/9-GALC alone) was composed of 31 animals (25 for lifespan, behavior, and terminal histology; 3 for 36-day biochemistry and histology; and 3 for 36-day cytokine analysis). The 3xRx WT group was composed of 25 animals (19 for lifespan, behavior, and terminal histology; 3 for 36-day biochemistry and histology; and 3 for 36-day cytokine analysis). The untreated Twi group was composed of 16 animals (10 for lifespan, behavior, and terminal histology; 3 for 36-day biochemistry and histology; and 3 for 36-day cytokine analysis). Finally, the untreated WT group was composed of 17 animals (11 for lifespan, behavior, and terminal histology; 3 for 36-day biochemistry and histology; and 3 for 36-day cytokine analysis).

Virus Production

The AAV2/9-GALC vector consists of the CMV enhancer and the chicken β-actin promoter, followed by the mouse *GALC* cDNA and the rabbit β-globin polyadenylation signal, as previously described.[51] The AAV2/9-GALC vector was produced by the Virus Vector Core Facility at the Gene Therapy Center of the University of North Carolina as a single-stranded AAV. Briefly, the virus was produced by tri- ple transfection of HEK293T cells. The cells were lysed and virus purified by sequential iodixanol step gradient centrifugation followed by anion exchange column chromatography. The virus was diluted in sterile Lactated Ringer's solution to a final concentration of 10^{12} viral particles per mL and stored at $-80°C$.

Treatment Regimen

IC and IT injections of AAV2/9-GALC were administered on postnatal day 0, as previously described.[16] Briefly, mice received one 15 μL IT injection of the virus at a concentration of 10^{12} viral particles per mL. In addition, six 2 μL IC injections were administered at the same concentration, targeting bilateral cortical hemispheres, thalami, and cerebelli. Therefore, the total dose of vector is approximately 2.7×10^{10} vg/pup (~2.7×10^{13} vg/kg).

HSCT was performed on postnatal day 1, as previously described.[16] Briefly, mice were conditioned with 400 rads total body irradiation from a ^{137}Cs source and then injected with 10^6 nucleated donor bone-marrow cells from a $GALC^{+/+}GFP^{+/-}$ donor.[52] Quantification of bone-marrow chimerism was determined by flow cytometry for donor-derived GFP expression in recipient bone marrow. Briefly, data were acquired using CellQuest software (BD Biosciences) and analyzed using FlowJo software (Tree Star). Gates were established
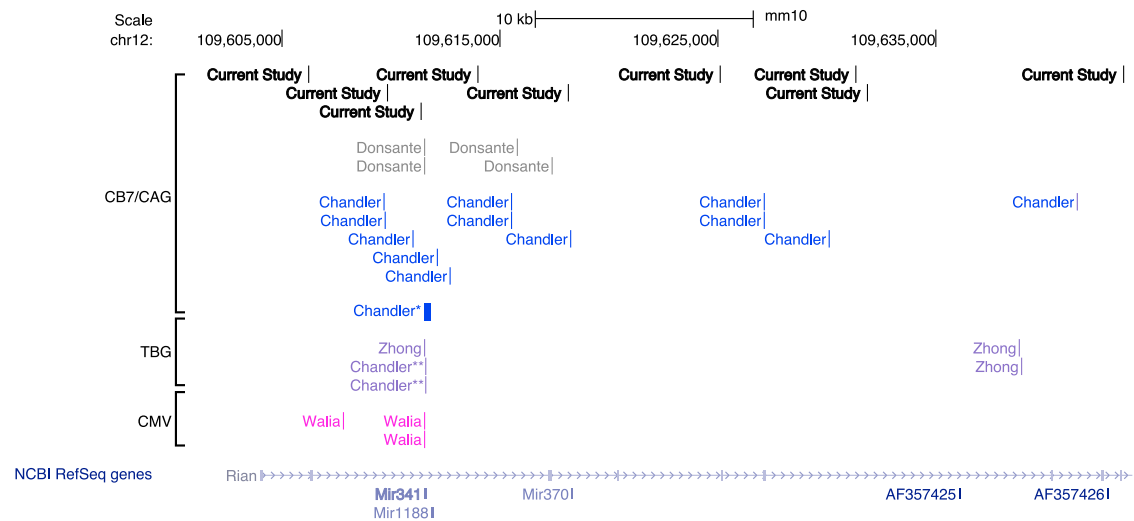
Figure 7. Pattern of Genotoxic AAV Integrations into RIAN

The genomic locations (UCSC Genome Browser, Genome Reference Consortium Mouse Build 38 December 2012, mm10) on chromosome 12 of rAAV HCC integrations in the Rian locus identified by previous studies[19–21] in comparison to those identified in the current study. Many of these integrations are within or near the *miR-341* locus, which is 96 base pairs in length. The thick bar designated by Chandler* represents 19 integrations that are within this locus. Junctions designated by Chandler** arise from a vector with a TBG promotor.

on nucleated bone-marrow cells from a GFP-positive donor animal to exclude dead cells and debris. The same gates were used to analyze nucleated bone-marrow cells from the recipient animals.

L-cycloserine was administered subcutaneously as previously described.[16] Briefly, L-cyloserine was reconstituted fresh in phosphate-buffered saline before each injection. Mice received 25 mg/kg L-cycloserine three times per week until postnatal day 28 and 50 mg/kg L-cycloserine three times per week for the rest of their lives.

GALC Activity Assay

Experimental mice were deeply anesthetized and perfused with phosphate-buffered saline. One brain hemisphere was flash frozen and homogenized in double-distilled H_2O (ddH_2O). Measurement of GALC activity was performed using a ³H-galactosylceramide substrate and reported as the nanomoles of substrate cleaved per hour per milligram of total protein, as previously described.[16]

Mass Spectrometry

Galactosylsphingosine (psychosine) and ceramides were measured in the brain, liver, and sciatic nerve as previously described.[53,54] Galactosylsphingosine was separated from glucosylsphingosine and glucosylceramide by hydrophilic interaction liquid chromatography (HILIC) columns. Ceramides were separated on two-dimensional chromatography by the HILIC column in the first dimension and by reversed phase column in the second dimension. Multiple reaction monitoring (MRM) was used to detect galactosylsphingosine and ceramides on an AB SCIEX 4000QTRAP tandem mass spectrometer in positive ESI mode. Data processing was conducted with Analyst 1.5.2 (Applied Biosystems). Data are reported as the peak area ratios of lipids to their internal standards.

Behavioral Testing

Behavioral testing consisted of the rotarod and wirehang tests, which were conducted as previously reported.[16] Mice were tested once every other week on the rotarod and once every week on the wirehang. Performance was measured as the time it took for the mouse to fall from either apparatus. Three trials were run and the average of the three trials was reported for each time point. For both tests, the maximum tested time was 60 s. Each group contained at least n = 10 animals.

Immunohistochemistry

Mice were deeply anesthetized and perfused with phosphate-buffered saline. One sagittal half of each brain was harvested immediately following perfusion. Tissues were fixed in 4% paraformaldehyde for 24–48 h at 4°C and cryoprotected in 30% sucrose. 16 μm sections were blocked in normal goat serum then incubated with primary rat anti-mouse CD68 (Bio-Rad), as previously described.[14] The sections were then incubated in the appropriate horseradish-peroxidase-conjugated secondary antibody and developed with a commercially available 3,3'-diaminobenzidine tetrahydrochloride (DAB) kit (Vector Laboratories).

Histology

Sciatic nerves were isolated and immediately fixed in 4% paraformaldehyde/2% glutaraldehyde. Incubation of nerves in osmium tetroxide was quickly followed by serial dehydration in ethanol and embedding in Araldite 502 (Polysciences). 1-μm-thick cross sections were prepared using an ultramicrotome. These sections were then stained with 1% toluidine blue and mounted on slides. Three random digital images of sciatic nerve cross sections for each animal were obtained at 100× magnification. Myelinated axons were then counted within

each field (102 μm^2 area) by an observer blinded to genotype and treatment, and the data for each of the three fields were tabulated for statistical comparison. Image acquisition was completed with a Hitachi CCD KP-MIAN digitizing camera mounted on a Leitz Laborlux S microscope. The Leco IA32 Image Analysis System was used for histomorphometric analysis.

Cytokine Measurement

Brains were perfused with phosphate-buffered saline, followed by immediate flash freezing and homogenization in a solution containing protease inhibitor cocktail. Cytokine levels were quantified using the Bio-plex Pro Mouse Cytokine 23-plex Assay (Bio-Rad) with the help of Dr. Camaron Hole and the Doering Lab at Washington University in St. Louis.

Statistical Analysis

Statistical significance was calculated using a one-way ANOVA with post hoc Bonferroni correction for multiple comparisons, unless otherwise specified. The p values are denoted as follows: $*p < 0.05$; $**p < 0.01$; $***p < 0.001$; ns denotes not significant, $p \geq 0.05$.

Sequence Production and Analysis

Genomic DNA was isolated, captured using 82 probes ordered from IDT to target the AAV vector, and sequenced on an Illumina NovaSeq 6000. Reads were aligned using BWA mem version 0.7.15,[34,35,36,55] and duplicates were marked with Picard version 2.18.1. Non-duplicated reads with one end mapping to the AAV construct and the other to the genome were retained. Regions of 1,000 bp with at least 25 reads were extracted in each sample. Such sites found in greater than 50% of samples were removed as artifacts, and then only tumor-specific (absent in the matched normal) sites with at least 50 unique reads of evidence were retained. Each site was manually reviewed to remove additional alignment artifacts or those with recurrent peaks in every sample. The *Galc* locus was also excluded from the integration site list due to its presence in the vector sequence.

SUPPLEMENTAL INFORMATION

Supplemental Information can be found online at https://doi.org/10.1016/j.ymthe.2020.12.031.

AUTHOR CONTRIBUTIONS

Y.L. and M.S.S. conceived the study and prepared the manuscript. Y.L., C.A.M., L.K.S., X.J., S.M.R., M.A.G., R.J.C., and S.N.S. performed critical experiments. T.J.L., C.A.V., C.P.V., and D.S.O. provided expert advice and/or novel reagents.

DECLARATION OF INTERESTS

The authors declare no competing interests.

REFERENCES

1. Krabbe, K. (1916). A new familial, infantile form of diffuse brain-sclerosis. Brain *39*, 74–114.

2. Wenger, D.A., Rafi, M.A., and Luzi, P. (2016). Krabbe disease: One Hundred years from the bedside to the bench to the bedside. J. Neurosci. Res. *94*, 982–989.

3. Wright, M.D., Poe, M.D., DeRenzo, A., Haldal, S., and Escolar, M.L. (2017). Developmental outcomes of cord blood transplantation for Krabbe disease: A 15-year study. Neurology *89*, 1365–1372.

4. Duchen, L.W., Eicher, E.M., Jacobs, J.M., Scaravilli, F., and Teixeira, F. (1980). Hereditary leucodystrophy in the mouse: the new mutant twitcher. Brain *103*, 695–710.

5. Kobayashi, T., Yamanaka, T., Jacobs, J.M., Teixeira, F., and Suzuki, K. (1980). The Twitcher mouse: an enzymatically authentic model of human globoid cell leukodystrophy (Krabbe disease). Brain Res. *202*, 479–483.

6. Hawkins-Salsbury, J.A., Reddy, A.S., and Sands, M.S. (2011). Combination therapies for lysosomal storage disease: is the whole greater than the sum of its parts? Hum. Mol. Genet. *20* (R1), R54–R60.

7. Li, Y., and Sands, M.S. (2014). Experimental therapies in the murine model of globoid cell leukodystrophy. Pediatr. Neurol. *51*, 600–606.

8. Mikulka, C.R., and Sands, M.S. (2016). Treatment for Krabbe's disease: Finding the combination. J. Neurosci. Res. *94*, 1126–1137.

9. Biswas, S., and LeVine, S.M. (2002). Substrate-reduction therapy enhances the benefits of bone marrow transplantation in young mice with globoid cell leukodystrophy. Pediatr. Res. *51*, 40–47.

10. Lin, D., Donsante, A., Macauley, S., Levy, B., Vogler, C., and Sands, M.S. (2007). Central nervous system-directed AAV2/5-mediated gene therapy synergizes with bone marrow transplantation in the murine model of globoid-cell leukodystrophy. Mol. Ther. *15*, 44–52.

11. Rafi, M.A., Rao, H.Z., Luzi, P., and Wenger, D.A. (2015). Long-term improvements in lifespan and pathology in CNS and PNS after BMT plus one intravenous injection of AAVrh10-GALC in Twitcher mice. Mol. Ther. *23*, 1681–1690.

12. Ricca, A., Rufo, N., Ungari, S., Morena, F., Martino, S., Kulik, W., Alberizzi, V., Bolino, A., Bianchi, F., Del Carro, U., et al. (2015). Combined gene/cell therapies provide long-term and pervasive rescue of multiple pathological symptoms in a murine model of globoid cell leukodystrophy. Hum. Mol. Genet. *24*, 3372–3389.

13. Karumuthil-Melethil, S., Marshall, M.S., Heindel, C., Jakubauskas, B., Bongarzone, E.R., and Gray, S.J. (2016). Intrathecal administration of AAV/GALC vectors in 10-11-day-old twitcher mice improves survival and is enhanced by bone marrow transplant. J. Neurosci. Res. *94*, 1138–1151.

14. Reddy, A.S., Kim, J.H., Hawkins-Salsbury, J.A., Macauley, S.L., Tracy, E.T., Vogler, C.A., Han, X., Song, S.K., Wozniak, D.F., Fowler, S.C., et al. (2011). Bone marrow transplantation augments the effect of brain- and spinal-cord-directed AAV 2/5 gene therapy by altering inflammation in the murine model of GLD. J. Neurosci. *31*, 9945–9957.

15. Sundaram, K.S., and Lev, M. (1984). Inhibition of sphingolipid synthesis by cycloserine in vitro and in vivo. J. Neurochem. *42*, 577–581.

16. Hawkins-Salsbury, J.A., Shea, L., Jiang, X., Hunter, D.A., Guzman, A.M., Reddy, A.S., Qin, E.Y., Li, Y., Gray, S.J., Ory, D.S., and Sands, M.S. (2015). Mechanism-based combination treatment dramatically increases therapeutic efficacy in murine globoid cell leukodystrophy. J. Neurosci. *35*, 6495–6505.

17. Cearley, C.N., and Wolfe, J.H. (2006). Transduction characteristics of adeno-associated virus vectors expressing cap serotypes 7, 8, 9, and Rh10 in the mouse brain. Mol. Ther. *13*, 528–537.

18. Donsante, A., Vogler, C., Muzyczka, N., Crawford, J.M., Barker, J., Flotte, T., Campbell-Thompson, M., Daly, T., and Sands, M.S. (2001). Observed incidence of tumorigenesis in long-term rodent studies of rAAV vectors. Gene Ther. *8*, 1343–1346.

19. Donsante, A., Miller, D.G., Li, Y., Vogler, C., Brunt, E.M., Russell, D.W., and Sands, M.S. (2007). AAV vector integration sites in mouse hepatocellular carcinoma. Science 317, 477.

20. Chandler, R.J., LaFave, M.C., Varshney, G.K., Trivedi, N.S., Carrillo-Carrasco, N., Senac, J.S., Wu, W., Hoffmann, V., Elkahloun, A.G., Burgess, S.M., and Venditti, C.P. (2015). Vector design influences hepatic genotoxicity after adeno-associated virus gene therapy. J. Clin. Invest. 125, 870–880.

21. Walia, J.S., Altaleb, N., Bello, A., Kruck, C., LaFave, M.C., Varshney, G.K., Burgess, S.M., Chowdhury, B., Hurlbut, D., Hemming, R., et al. (2015). Long-term correction of Sandhoff disease following intravenous delivery of rAAV9 to mouse neonates. Mol. Ther. 23, 414–422.

22. Knudson, A.G., Jr. (1971). Mutation and cancer: statistical study of retinoblastoma. Proc. Natl. Acad. Sci. USA 68, 820–823.

23. Koybasi, S., Senkal, C.E., Sundararaj, K., Spassieva, S., Bielawski, J., Osta, W., Day, T.A., Jiang, J.C., Jazwinski, S.M., Hannun, Y.A., et al. (2004). Defects in cell growth regulation by C18:0-ceramide and longevity assurance gene 1 in human head and neck squamous cell carcinomas. J. Biol. Chem. 279, 44311–44319.

24. Yang, J., Tian, Y., Zheng, R., Li, L., and Qiu, F. (2019). Endocannabinoid system and the expression of endogenous ceramides in human hepatocellular carcinoma. Oncol. Lett. 18, 1530–1538.

25. Molee, P., Adisakwattana, P., Reamtong, O., Petmitr, S., Sricharunrat, T., Suwandittakul, N., and Chaisri, U. (2015). Up-regulation of AKAP13 and MAGT1 on cytoplasmic membrane in progressive hepatocellular carcinoma: a novel target for prognosis. Int. J. Clin. Exp. Pathol. 8, 9796–9811.

26. Chen, J., Xuan, Z., Song, W., Han, W., Chen, H., Du, Y., Xie, H., Zhao, Y., Zheng, S., and Song, P. (2020). EAG1 enhances hepatocellular carcinoma proliferation by modulating SKP2 and metastasis through pseudopod formation. Oncogene. Published online October 24, 2020. https://doi.org/10.1038/s41388-020-01522-6.

27. Yang, J., Wang, B., Xu, Q., Yang, Y., Hou, L., Yin, K., Guo, Q., Hua, Y., Zhang, L., Li, Y., Zhang, J., and Li, N. (2020). TMEM166 inhibits cell proliferation, migration, and invasion in hepatocellular carcinoma via upregulating TP53. Mol Cell Biochem. Published online November 16, 2020. https://doi.org/10.1007/s11010-020-03979-1.

28. Xiao, J., He, B., Zou, Y., Chen, X., Lu, X., Xie, M., Li, W., He, S., You, S., and Chen, Q. (2016). Prognostic value of decreased FOXP1 protein expression in various tumors: a systematic review and meta-analysis. Sci. Rep. 6, 30437.

29. Zhang, Y., Zhang, S., Wang, X., Liu, J., Yang, L., He, S., Chen, L., and Huang, J. (2012). Prognostic significance of FOXP1 as an oncogene in hepatocellular carcinoma. J. Clin. Pathol. 65, 528–533.

30. Sheng, X.R., Xing, S.G., Wang, R.D., Chen, K., and Jia, W.D. (2018). Low levels of tumor suppressor candidate 3 predict poor prognosis of patients with hepatocellular carcinoma. OncoTargets Ther. 11, 909–917.

31. Alday-Parejo, B., Richard, F., Wörthmüller, J., Rau, T., Galván, J.A., Desmedt, C., Santamaria-Martinez, A., and Rüegg, C. (2020). Magi1, a new potential tumor suppressor gene in estrogen receptor positive breast cancer. Cancers (Basel) 12, 223.

32. Zhang, G., Liu, T., and Wang, Z. (2012). Downregulation of MAGI1 associates with poor prognosis of hepatocellular carcinoma. J. Invest. Surg. 25, 93–99.

33. Wang, P.R., Xu, M., Toffanin, S., Li, Y., Llovet, J.M., and Russell, D.W. (2012). Induction of hepatocellular carcinoma by in vivo gene targeting. Proc. Natl. Acad. Sci. USA 109, 11264–11269.

34. Bentin Toaldo, C., Alexi, X., Beelen, K., Kok, M., Hauptmann, M., Jansen, M., Berns, E., Neefjes, J., Linn, S., Michalides, R., and Zwart, W. (2015). Protein Kinase A-induced tamoxifen resistance is mediated by anchoring protein AKAP13. BMC Cancer 15, 588.

35. Cázares-Ordoñez, V., and Pardo, L.A. (2017). Kv10.1 potassium channel: from the brain to the tumors. Biochem. Cell Biol. 95, 531–536.

36. Shen, X., Kan, S., Liu, Z., Lu, G., Zhang, X., Chen, Y., and Bai, Y. (2017). EVA1A inhibits GBM cell proliferation by inducing autophagy and apoptosis. Exp. Cell Res. 352, 130–138.

37. Bradbury, A.M., Rafi, M.A., Bagel, J.H., Brisson, B.K., Marshall, M.S., Pesayco Salvador, J., Jiang, X., Swain, G.P., Prociuk, M.L., ODonnell, P.A., et al. (2018). AAVrh10 gene therapy ameliorates central and peripheral nervous system disease in canine globoid cell leukodystrophy (Krabbe Disease). Hum. Gene Ther. 29, 785–801.

38. Meneghini, V., Lattanzi, A., Tiradani, L., Bravo, G., Morena, F., Sanvito, F., Calabria, A., Bringas, J., Fisher-Perkins, J.M., Dufour, J.P., et al. (2016). Pervasive supply of therapeutic lysosomal enzymes in the CNS of normal and Krabbe-affected non-human primates by intracerebral lentiviral gene therapy. EMBO Mol. Med. 8, 489–510.

39. Marshall, M.S., Issa, Y., Jakubauskas, B., Stoskute, M., Elackattu, V., Marshall, J.N., Bogue, W., Nguyen, D., Hauck, Z., Rue, E., et al. (2018). Long-term improvement of neurological signs and metabolic dysfunction in a mouse model of Krabbe's disease after global gene therapy. Mol. Ther. 26, 874–889.

40. Snook, E.R., Fisher-Perkins, J.M., Sansing, H.A., Lee, K.M., Alvarez, X., MacLean, A.G., Peterson, K.E., Lackner, A.A., and Bunnell, B.A. (2014). Innate immune activation in the pathogenesis of a murine model of globoid cell leukodystrophy. Am. J. Pathol. 184, 382–396.

41. Santambrogio, S., Ricca, A., Maderna, C., Ieraci, A., Aureli, M., Sonnino, S., Kulik, W., Aimar, P., Bonfanti, L., Martino, S., and Gritti, A. (2012). The galactocerebrosidase enzyme contributes to maintain a functional neurogenic niche during early post-natal CNS development. Hum. Mol. Genet. 21, 4732–4750.

42. Potter, G.B., and Petryniak, M.A. (2016). Neuroimmune mechanisms in Krabbe's disease. J. Neurosci. Res. 94, 1341–1348.

43. Chandler, R.J., LaFave, M.C., Varshney, G.K., Burgess, S.M., and Venditti, C.P. (2016). Genotoxicity in mice following AAV gene delivery: a safety concern for human gene therapy? Mol. Ther. 24, 198–201.

44. Gray, S.J., Nagabhushan Kalburgi, S., McCown, T.J., and Jude Samulski, R. (2013). Global CNS gene delivery and evasion of anti-AAV-neutralizing antibodies by intrathecal AAV administration in non-human primates. Gene Ther. 20, 450–459.

45. Meyer, K., Ferraiuolo, L., Schmelzer, L., Braun, L., McGovern, V., Likhite, S., Michels, O., Govoni, A., Fitzgerald, J., Morales, P., et al. (2015). Improving single injection CSF delivery of AAV9-mediated gene therapy for SMA: a dose-response study in mice and nonhuman primates. Mol. Ther. 23, 477–487.

46. Zincarelli, C., Soltys, S., Rengo, G., and Rabinowitz, J.E. (2008). Analysis of AAV serotypes 1-9 mediated gene expression and tropism in mice after systemic injection. Mol. Ther. 16, 1073–1080.

47. Adewoye, A.B., Lindsay, S.J., Dubrova, Y.E., and Hurles, M.E. (2015). The genome-wide effects of ionizing radiation on mutation induction in the mammalian germline. Nat. Commun. 6, 6684.

48. Hordeaux, J., Buza, E.L., Dyer, C., Goode, T., Mitchell, T.W., Richman, L., Denton, N., Hinderer, C., Katz, N., Schmid, R., et al. (2020). Adeno-associated virus-induced dorsal root ganglion pathology. Hum. Gene Ther. 31, 808–818.

49. Nault, J.C., Datta, S., Imbeaud, S., Franconi, A., Mallet, M., Couchy, G., Letouzé, E., Pilati, C., Verret, B., Blanc, J.F., et al. (2015). Recurrent AAV2-related insertional mutagenesis in human hepatocellular carcinomas. Nat. Genet. 47, 1187–1193.

50. Sakai, N., Inui, K., Tatsumi, N., Fukushima, H., Nishigaki, T., Taniike, M., Nishimoto, J., Tsukamoto, H., Yanagihara, I., Ozono, K., and Okada, S. (1996). Molecular cloning and expression of cDNA for murine galactocerebrosidase and mutation analysis of the twitcher mouse, a model of Krabbe's disease. J. Neurochem. 66, 1118–1124.

51. Lin, D., Fantz, C.R., Levy, B., Rafi, M.A., Vogler, C., Wenger, D.A., and Sands, M.S. (2005). AAV2/5 vector expressing galactocerebrosidase ameliorates CNS disease in the murine model of globoid-cell leukodystrophy more efficiently than AAV2. Mol. Ther. 12, 422–430.

52. Okabe, M., Ikawa, M., Kominami, K., Nakanishi, T., and Nishimune, Y. (1997). 'Green mice' as a source of ubiquitous green cells. FEBS Lett. 407, 313–319.

53. Sikora, J., Dworski, S., Jones, E.E., Kamani, M.A., Micsenyi, M.C., Sawada, T., Le Faouder, P., Bertrand-Michel, J., Dupuy, A., Dunn, C.K., et al. (2017). Acid ceramidase deficiency in mice results in a broad range of central nervous system abnormalities. Am. J. Pathol. 187, 864–883.

54. Sidhu, R., Mikulka, C.R., Fujiwara, H., Sands, M.S., Schaffer, J.E., Ory, D.S., and Jiang, X. (2018). A HILIC-MS/MS method for simultaneous quantification of the lysosomal disease markers galactosylsphingosine and glucosylsphingosine in mouse serum. Biomed. Chromatogr. 32, e4235.

55. Li, H. (2013). Aligning sequence reads, clone sequences and assembly contigs with BWA-MEM. arXiv, arXiv:13033997, https://arxiv.org/abs/1303.3997.

Supplemental Information

Enhanced Efficacy and Increased

Long-Term Toxicity of CNS-Directed, AAV-Based

Combination Therapy for Krabbe Disease

Yedda Li, Christopher A. Miller, Lauren K. Shea, Xuntian Jiang, Miguel A. Guzman, Randy J. Chandler, Sai M. Ramakrishnan, Stephanie N. Smith, Charles P. Venditti, Carole A. Vogler, Daniel S. Ory, Timothy J. Ley, and Mark S. Sands

Supplemental Table 1:

Locations of all reported AAV integration sites into the mouse genome, along with the total number of reads supporting the site and gene intersections (includes introns and UTR).

animal#	chromosome	position	supporting_reads	gene_id	gene_name
6657	12	109641315	277	ENSMUSG00000097451	*Rian*
6657	12	109643597	884	ENSMUSG00000097451	*Rian*
6675	1	24600881	65		
6675	1	64997657	181		
6675	10	20168402	51	ENSMUSG00000019996	*Map7*
6675	10	121735894	52		
6675	12	59192057	163		
6675	12	65081934	70	ENSMUSG00000055884	*Fancm*
6675	12	102796969	108	ENSMUSG00000041702	*Btbd7*
6675	12	109618074	1389	ENSMUSG00000097451	*Rian*
6675	18	36546602	77		
6675	19	17071550	828	ENSMUSG00000039126	*Prune2*
6675	19	23079959	51		
6675	2	69855356	282		
6675	2	140076919	63		
6675	3	18079127	61	ENSMUSG00000039519	*Cyp7b1*
6675	4	32888006	138	ENSMUSG00000040183	*Ankrd6*
6675	4	66989476	55		
6675	4	116827537	204	ENSMUSG00000086417	*Gm12996*
6675	4	126795906	73	ENSMUSG00000028830	*AU040320*
6675	4	133924782	165		
6675	4	136309554	159		
6675	5	26686746	58		
6675	5	126622362	86		
6675	5	127258665	61	ENSMUSG00000034324	*Tmem132c*
6675	6	36943263	66	ENSMUSG00000038665	*Dgki*
6675	6	45023809	197		
6675	6	99149868	2879	ENSMUSG00000030067	*Foxp1*
6675	8	4494995	53	ENSMUSG00000008206	*Cers4*
6675	8	39104763	167	ENSMUSG00000039530	*Tusc3*
6675	8	123487614	146	ENSMUSG00000031967	*Afg3l1*
6675	9	108268425	11407		
6722	12	109631712	1499	ENSMUSG00000097451	*Rian*
6722	2	6422180	1282	ENSMUSG00000039046	*Usp6nl*
6722	7	75627402	880	ENSMUSG00000066406	*Akap13*
6815	12	109609803	1658	ENSMUSG00000097451	*Rian*

6824	1	73981261	63	ENSMUSG00000055322	Tns1
6824	1	192215898	149	ENSMUSG00000058248	Kcnh1
6824	10	56888871	107		
6824	12	109631227	609	ENSMUSG00000097451	Rian
6824	6	81973046	83		
6824	Y	3990091	76		
6828	12	109625076	2056	ENSMUSG00000097451	Rian
6828	5	58355670	53		
6828	5	91978136	63		
6828	7	13465551	92	ENSMUSG00000074378	Bsph1
6828	7	122053066	54	ENSMUSG00000030871	Ears2
6902	12	109671965	410	ENSMUSG00000102657	Gm37899
6902	2	7965507	77		
6902	6	94142817	54	ENSMUSG00000045095	Magi1
6902	9	25074525	87		
7025	10	11676011	2091		
7025	10	13470373	75	ENSMUSG00000062866	Phactr2
7025	12	109614971	1430	ENSMUSG00000097451	Rian
7025	4	145837135	369		
7025	4	147187698	167	ENSMUSG00000097168	C230088H06Rik
7025	7	75787121	59		
7025	7	100533860	84		
7025	9	111682793	1659	ENSMUSG00000032502	Stac
7045	12	109606204	1853	ENSMUSG00000097451	Rian
7046	11	3208037	446	ENSMUSG00000020457	Drg1
7046	12	6577831	80		
7046	12	58759516	115		
7046	12	109611352	411	ENSMUSG00000097451	Rian
7046	14	20052930	220		
7046	15	86614767	69		
7046	17	32319795	79	ENSMUSG00000024045	Akap8
7046	18	10686802	279	ENSMUSG00000002475	Abhd3
7046	3	35237902	447		
7046	3	82861889	1431	ENSMUSG00000033882	Rbm46
7046	5	135257207	79		
7046	7	127555881	164	ENSMUSG00000053877	Srcap
7046	8	124886315	1859	ENSMUSG00000031985	Gnpat

Supplemental Table 2: Rian integration site assembly
The softclipped portion of reads crossing the *Rian* locus breakpoints were aligned against the AAV vector sequence to determine what portion of the vector was integrated, when possible
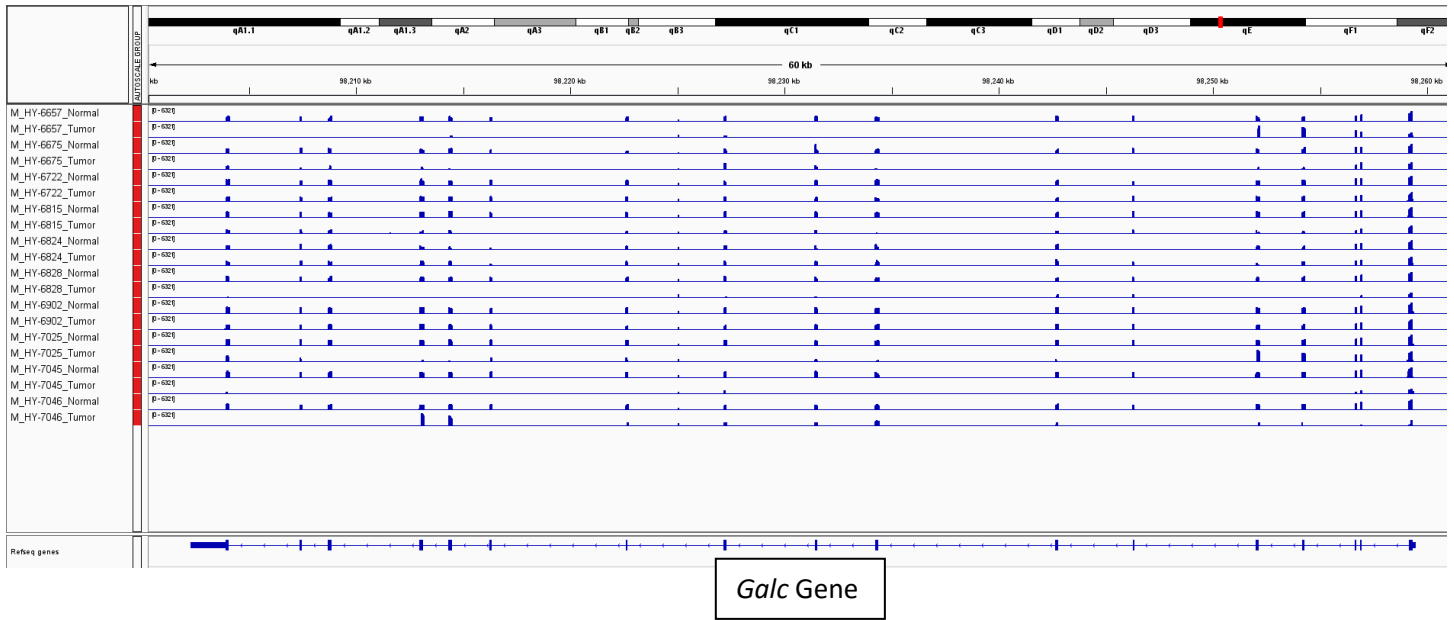
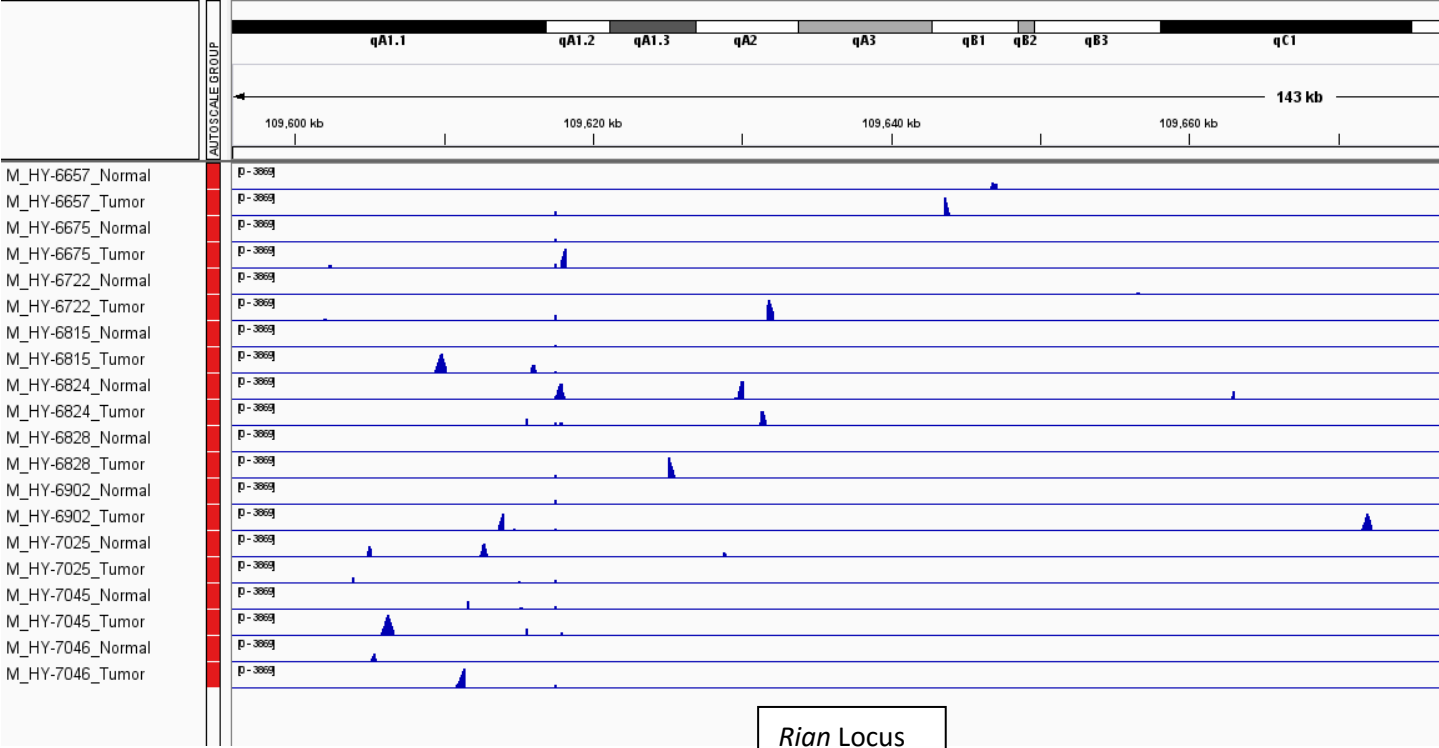| Animal #	Vector breakpoints
6657	433, 2008
6675	690 (no other end)
6722	222, 1520
6815	183, 916, 4685 (complex)
6824	276, 1531
6828	224, 4724
6902	222, 1756, 4726 (complex)
6902	222, 893
7025	1570, 4459, 4756 (complex)
7045	209, 655, 4739 (complex)
7046	735, 4756

Supplemental Figures

Supplemental Figure 1. Targeted sequence capture correctly identifies the murine *GALC* gene. The targeted sequence capture probes that span the AAV2/9-GALC ITRs, CAGGS promoter, and the human GALC cDNA identify nearly every exon in the murine *Galc* gene in both normal and tumor tissue. This serves as a positive control for the sequencing probes. The vertical blue bars show the relative read counts. The individual animal numbers and whether it is tumor or normal tissue are listed to the left of the read counts. The *Galc* gene exon/intron structure is shown below the read counts.

Supplemental Figure 2. Targeted sequence capture identified AAV integration sites in 3xRx WT mice. (A) The relative read counts for AAV integrations into the *Rian* locus in tumor samples are shown as vertical blue peaks. **(B)** The relative read counts for the AAV integration site in the *Foxp1* tumor suppressor gene in animal number 6675 are shown. **(C)** The relative read counts for the AAV integration site in the candidate tumor suppressor gene *Magi1* in animal number 6902 are shown. **(D)** The relative read counts for the AAV integration site in the *Eva1a* gene in animal number 6815 are shown. **(E)** The relative read counts for the AAV integration site in the *Kcnh1* gene in animal number 6824 are shown. **(F)** The relative read counts for the AAV integration site in the candidate tumor suppressor gene *Tusc3* in animal number 6675 are shown. **(G)** The relative read counts for the Akap13 gene in animal number 6722 are shown. In each case, the individual animal number and chromosomal position (bp) are shown to the left and top of the plots, respectively.
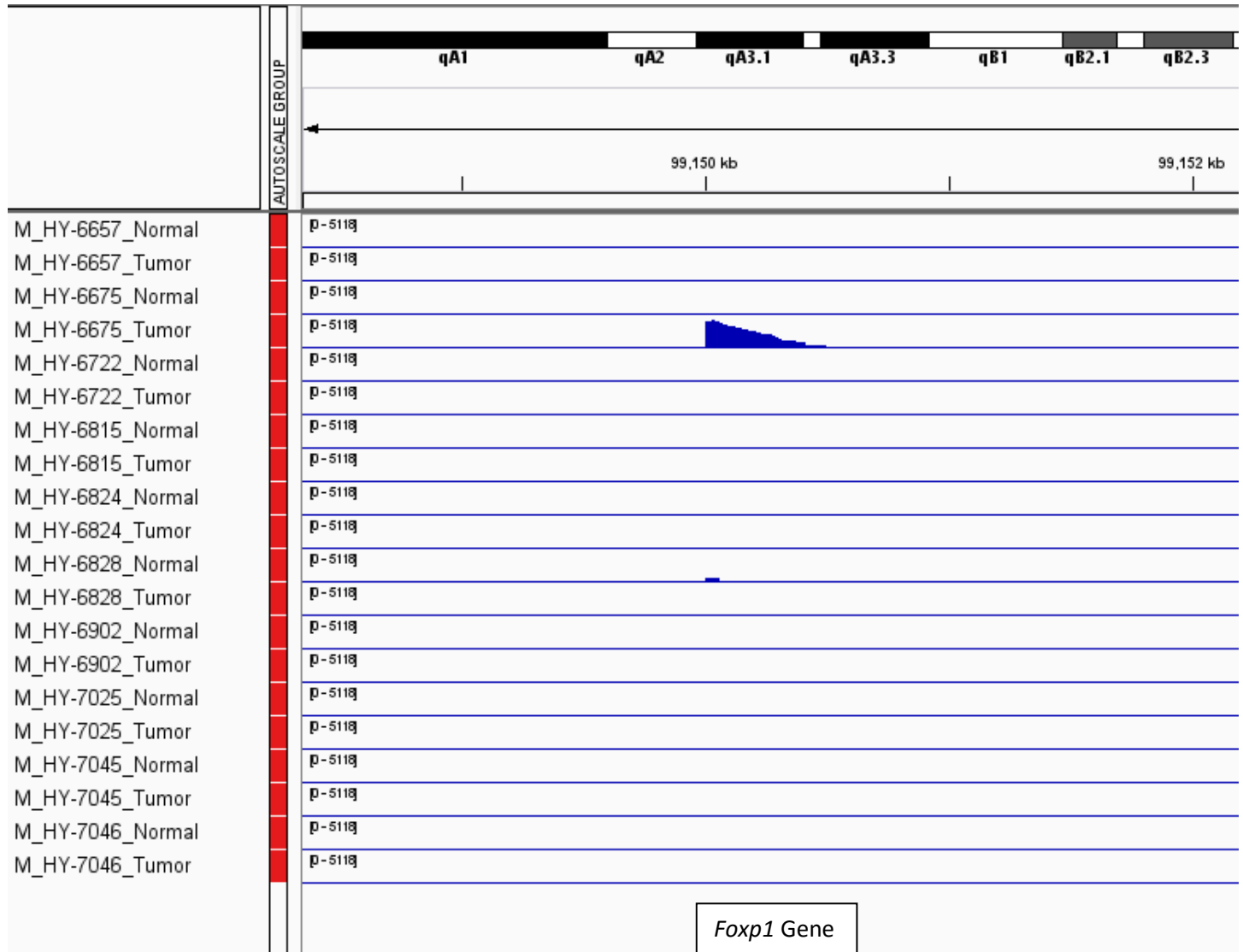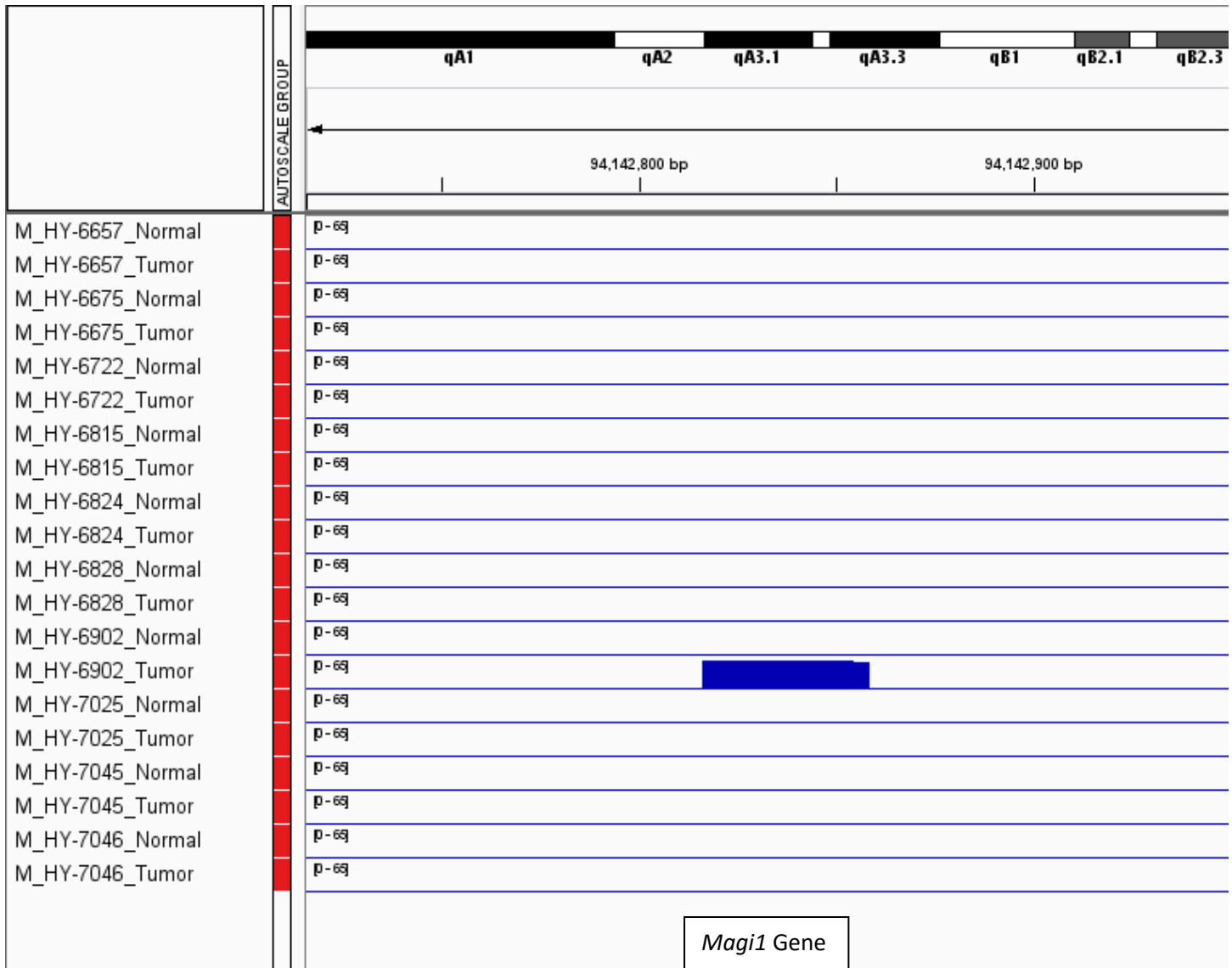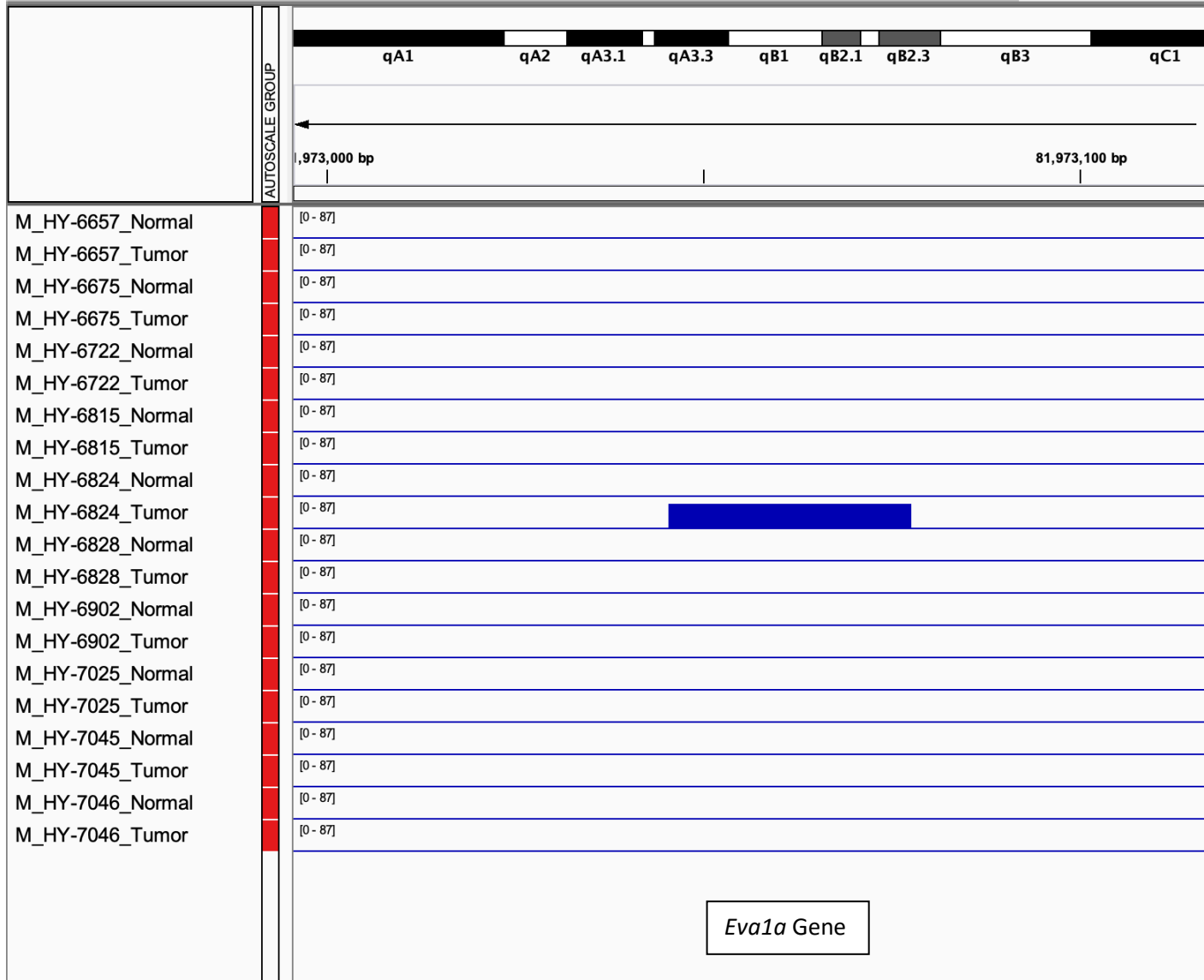
Supplemental Figure 1.

Galc Gene

Supplemental Figure 2A.

Rian Locus

Supplemental Figure 2B.

Foxp1 Gene

Supplemental Figure 2C.

Magi1 Gene

Supplemental Figure 2D.

Eva1a Gene

Supplemental Figure 2E.

Kcnh1 Gene

Supplemental Figure 2F.

Tusc3 Gene

Akap13 Gene